Stationary phase evaluations of quantum rate constants

Shilong Yang and Jianshu Cao[a)]
Department of Chemistry, Massachusetts Institute of Technology, Cambridge, Massachusetts 02139

(Received 25 October 2004; accepted 14 December 2004; published online 1 March 2005)

We compute the quantum rate constant based on two extended stationary phase approximations to the imaginary-time formulation of the quantum rate theory. The optimized stationary phase approximation to the imaginary-time flux-flux correlation function employs the optimized quadratic reference system to overcome the inaccuracy of the quadratic expansion in the standard stationary phase approximation, and yields favorable agreements with instanton results for both adiabatic and nonadiabatic processes in dissipative and nondissipative systems. The integrated stationary phase approximation to the two-dimensional barrier free energy is particularly useful for adiabatic processes and demonstrates consistent results with the imaginary-time flux-flux correlation function approach. Our stationary phase methods do not require calculation of tunneling paths or stability matrices, and work equally well in the high-temperature and the low-temperature regimes. The numerical results suggest their general applicability for calibration of imaginary-time methods and for the calculation of quantum rate constants in systems with a large number of degrees of freedom. © *2005 American Institute of Physics*. [DOI: 10.1063/1.1856461]

I. INTRODUCTION

The calculation of thermal rate constants for chemical reactions has been one of the most active areas in theoretical chemistry.[1] Through analytical continuation, the quantum dynamics calculation is mapped into quantum statistical mechanics, which has been implemented in a number of quantum, mixed quantum-classical, or semiclassical methods.[2–7] Of particular importance is the imaginary-time path-integral formulation of thermal averaged quantum tunneling rate, i.e., quantum rate constant. Two related concepts have appeared in literature: the imaginary-time flux-flux correlation function and the barrier partition function.

The imaginary-time flux-flux correlation function is numerically more feasible than the real-time flux-flux correlation function. Real-time correlation functions require intensive calculations of Feynman path integrals[8] and are difficult to converge. Numerical schemes proposed by Berne, Doll, and their co-workers are based on direct analytical continuation of imaginary-time correlation function.[9–13] Yet the analytical continuation from the imaginary-time to real time is numerically unstable, which is the major drawback of these schemes. Since the thermal rate constant is the zero-frequency component and does not require the information about the whole spectrum, the quantum reaction rate can be computed from the stationary phase approximation of the imaginary-time flux-flux correlation function. This method was proposed by Wolynes and yielded the Golden rule rate in the nonadiabatic limit.[5,6]

The barrier partition function concept relates the quantum reactive flux to the imaginary part of the barrier partition function.[14–17] The stationary phase approximations employed to calculate the barrier partition function distinguish different quantum rate theories. At high temperatures, the rate process is dominated by thermal activation and is described by transition state theory. Quantum mechanical corrections lead to modifications of classical transition state theory. The quantum transition state theory[18] (QTST) uses a parabolic barrier potential and the harmonic approximation to the rest of Fourier modes. The path-integral quantum transition state theory (PI-QTST) based on the centroid concept has a similar structure to that of classical TST except that the classical transition state is replaced by the centroid.[19,20] The mixed quantum-classical rate theory (MQCLT) transforms the evaluation of the reactive flux into the reduced phase space via the Wigner transform.[21] Both PI-QTST and MQCLT employ stationary phase approximations to the unstable mode. At low temperatures, the rate process is dominated by the tunneling effect, resulting in the nontrivial periodic stationary path, i.e., the instanton.[2,22,23] In the instanton approach, stationary phase approximations are employed to describe fluctuation modes around the instanton path. More recently, Miller and co-workers successfully applied the semiclassical stationary phase approximation with two dividing surfaces to quantum Boltzmann operator and reached excellent agreement with the exact results for one-dimensional (1D) and 2D systems.[4] Several theoretical attempts were proposed to bridge the imaginary-time flux-flux correlation function and the barrier partition function.[2,16,17,24] The instanton concept was originally introduced by Miller and has been widely applied to adiabatic processes. Cao and Voth proposed the nonadiabatic instanton approach,[24–26] where stationary phase approximation of the imaginary-time flux-flux correlation function in the nonadiabatic limit gave rise to an explicit form of the imaginary part of the barrier partition function. This nonadiabatic instanton approach calculates both the nonadiabatic electron-transfer rate and the adiabatic quantum tunneling rate over a broad range of coupling constants within the same framework.

[a)]Electronic mail: jianshu@mit.edu

In the present paper, we examine two stationary phase methods for computing quantum rate constants. The first method is derived from the optimized stationary phase approximation to the imaginary-time flux-flux correlation function, which applies the approach by Wolynes[5] to both adiabatic and nonadiabatic processes. Optimized quadratic approximation[27,28] is employed to overcome the inaccuracy of the quadratic expansion in the standard stationary phase approximation. In the second method, the imaginary part of the barrier partition function is calculated from the integrated stationary phase approximations to the spatial coordinates of the 2D barrier free energy surface. This method is motivated by the quantum Boltzmann operator calculated by Miller *et al.*[4] and is a generalization of the barrier partition function concept.[14–17] The 2D barrier free energy method is applicable to adiabatic processes where the 2D barrier free energy profile can be computed. A spatial integration scheme is proposed to enhance the accuracy of the stationary phase approximation. These two stationary phase methods do not require tunneling path calculations at low temperatures or quantum correction factors at high temperatures, and the imaginary-time dynamics can be computed with readily available numerical path-integral techniques.

Although both stationary phase methods have been explored respectively, their accuracy has yet to be established numerically and their consistency has yet to be demonstrated. The goal of this paper is to demonstrate the agreement between these two approaches for adiabatic processes and their agreements with the instanton approach for nonadiabatic processes. Our numerical calculation suggests that the optimized stationary phase approximation to the imaginary-time flux-flux correlation function is applicable to both adiabatic and nonadiabatic processes.

The rest of the paper is organized as follows. In Sec. II, we discuss the optimized imaginary-time stationary phase method, the 2D barrier free energy method, and the instanton approach. In Sec. III, we demonstrate the accuracy of these two stationary phase methods and their agreements with the instanton approach for adiabatic systems. Specifically we present results for a nondissipative 1D Eckart potential, a dissipative Eckart potential, and a dissipative double-well potential. In Sec. IV, we test the optimized stationary phase approximation to the imaginary-time flux-flux correlation function for a nonadiabatic system, i.e., the spin-boson Hamiltonian. The conclusion is presented in Sec. V.

II. METHODS

In this section, we apply several stationary phase approximations to evaluate the quantum rate. In the first approach, the quantum rate is computed from the optimized stationary phase approximation to the imaginary-time coordinate. Here we generalize Wolynes's approach by including anharmonicity. In the second approach, integrated stationary phase approximations are applied to the spatial coordinates on the 2D barrier free energy surface. Both methods originate from analytical continuation of the reactive flux correlation function $C_{fs}(t)$, and the relation is illustrated in Fig. 1. The nonadiabatic instanton analysis essentially rotates the stationary phase coordinate from the imaginary-time axis to the spatial axes, providing a bridge between these two stationary phase methods.

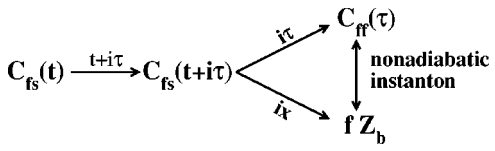

FIG. 1. Illustration of the relation between the barrier partition function concept, the imaginary-time flux-flux correlation function concept, and the nonadiabatic instanton approach.

A. Optimized stationary phase approximation to the imaginary-time flux-flux correlation function

In this section, we apply the approach by Wolynes[5] to both adiabatic and nonadiabatic cases by incorporating the non-Gaussian correction to the quadratic expansion used in the standard stationary phase approximation. The quantum flux operator is generally defined by

$$\hat{F} = \frac{i}{\hbar}[\hat{H}, \hat{h}_R], \tag{1}$$

where $\hat{h}_R$ is the occupation operator in the reactant state. The imaginary-time flux-flux correlation function is given by

$$C_{ff}(\tau) = \frac{1}{Z_r} \mathrm{Tr}\, e^{-\beta \hat{H}} \hat{F}(\tau) \hat{F}(0), \tag{2}$$

where $\hat{F}(\tau) = e^{H\tau} \hat{F} e^{-H\tau}$ is the imaginary-time flux operator and Z_r is the reactant partition function. Due to the cyclic property of trace function, this imaginary-time flux-flux correlation function is equivalent to the expression derived by Miller, Schwartz, and Tromp[3] after invoking the Wick's rotation $t \rightarrow i\tau$. The quantum rate is the time integral of the real-time correlation function, which becomes the imaginary part of the integral of the imaginary-time flux-flux correlation function, i.e.,

$$K = \tfrac{1}{2}\, \mathrm{Im} \int C_{ff}(\tau) d\tau. \tag{3}$$

The integral in Eq. (3) implies the stationary phase approximation to the imaginary-time and the quantum reactive flux is given by $F_{qm} = KZ_r$.

The evaluation of the quantum reaction rate depends on the accuracy of the stationary phase approximation. This issue becomes important at low temperatures, for example, for the double-well potential investigated in Sec. III B. It is also demonstrated in Sec. IV for the spin-boson model that the correlation function becomes flat at large electronic couplings. To achieve better accuracy, we employ a numerical implementation of the stationary phase approximation using the optimized quadratic approximation (OQA).[27,28] To proceed, we first write the imaginary-time flux-flux correlation as $C_{ff}(\tau) = \exp[-\Phi(\tau)]$, and expand $\Phi(\tau)$ at the stationary point τ_{st}, giving

$$\Phi(\tau) = \Phi(\tau_{st}) + \frac{1}{2}\Phi''(\tau_{st})(\tau - \tau_{st})^2 + \frac{1}{4!}\Phi^{(4)}(\tau_{st})(\tau - \tau_{st})^4 + \cdots. \quad (4)$$

The optimized quadratic potential reads $\Phi_{ref}(\tau) \approx \frac{1}{2}\alpha(\tau - \tau_{st})^2$ and the reference distribution is $[2\pi/\alpha]^{-1/2}\exp[-\alpha(\tau - \tau_{st})^2/2]$. Explicit average of the second derivative of the potential $\Phi(\tau)$ in Eq. (4) over the reference distribution leads to the optimized quadratic approximation

$$\alpha = \langle \Phi'' \rangle_\alpha \approx \Phi''(\tau_{st}) + \frac{\Phi^{(4)}(\tau_{st})}{2\alpha} \approx \Phi''(\tau_{st})\left(1 + \frac{\Phi^{(4)}(\tau_{st})}{2[\Phi''(\tau_{st})]^2}\right), \quad (5)$$

where the last expression is the leading order contribution of the optimized quadratic term and $\langle \cdots \rangle_\alpha$ represents the average over the optimized reference system. It is straightforward to show that $\Phi''(\tau_{st}) = C''_{ff}(\tau_{st})/C_{ff}(\tau_{st})$ and $\Phi^{(4)}(\tau_{st}) = C^{(4)}_{ff}(\tau_{st})/C_{ff}(\tau_{st}) - 3[C''_{ff}(\tau_{st})/C_{ff}(\tau_{st})]^2$. Hence, the quantum rate constant is given by

$$K = \int_0^\infty C_{ff}(\tau)d\tau \approx \left[\frac{1}{2}\left(\frac{C^{(4)}_{ff}(\tau_{st})/C_{ff}(\tau_{st})}{[C''_{ff}(\tau_{st})/C_{ff}(\tau_{st})]^2} - 1\right)\right]^{-1/2} \times \left[\frac{2\pi}{C''_{ff}(\tau_{st})/C_{ff}(\tau_{st})}\right]^{-1/2} C_{ff}(\tau_{st}), \quad (6)$$

where the first term is the non-Gaussian correction factor and the rest is the rate from stationary phase approximation.

The optimized stationary phase approximation to the imaginary-time flux-flux correlation function does not assume weak coupling, hence is equally applicable to the nonadiabatic limit, the adiabatic limit, and the intermediate region. The non-Gaussian correction factor incorporates the deviation from the standard quadratic approximation and makes the stationary phase method reliable for calculations of quantum rate constants over a broader range of temperatures. We illustrate these points in Secs. III and IV.

B. Integrated stationary phase approximation to the 2D barrier free energy

Another approach to compute quantum rate constants is using the barrier partition function concept. In this approach, the quantum reactive flux is expressed as a product of a simple frequency factor and the imaginary part of the barrier partition function,

$$F \simeq \nu \,\mathrm{Im}\, Z_b, \quad (7)$$

where Z_b is the partition function in the barrier region and ν is the temperature-dependent frequency factor. The barrier partition function is given by

$$Z_b = \mathrm{Tr}\, e^{-\beta H} = \int dq \int dq' \int D[q(\tau)] \int D[q'(\tau)] \times \exp\{-S[q(\tau),0,\beta/2] - S[q'(\tau),\beta/2,\beta]\}, \quad (8)$$

where $S[q(\tau),0,\beta/2] = \int_0^{\beta/2} H(\tau)d\tau$ is the Euclidean action functional of the path $q(\tau)$ from 0 to $\beta/2$. $\hbar$ is taken to be unity implicitly in the present paper unless otherwise specified. The functional integral is carried out over all the periodic paths of period $\hbar\beta$. For dissipative systems, the frequency factor is given by

$$\nu = \begin{cases} \lambda_0^\ddagger/2\pi, & \beta\hbar\lambda_0^\ddagger < 2\pi \\ 1/\hbar\beta, & \beta\hbar\lambda_0^\ddagger \geqslant 2\pi, \end{cases} \quad \text{with } \lambda_0^\ddagger = \frac{\omega_b^2}{\lambda_0^\ddagger + \hat{\eta}(\lambda_0^\ddagger)/m}. \quad (9)$$

Here m is the effective mass of the reaction coordinate and $\hat{\eta}(z)$ is the Laplace transform of the classical friction kernel at the top of the barrier. The crossover temperature is defined by $\beta\hbar\lambda_0^\ddagger = 2\pi$ with $\lambda_0^\ddagger$ the Grote–Hynes frequency.[29,30] For nondissipative systems, $\hat{\eta}(z) = 0$, and $\lambda_0^\ddagger$ reduces to ω_b. At high temperatures, the imaginary part of the barrier partition function arises from the stationary phase approximation to the unstable mode. At low temperatures, the imaginary part of the barrier partition function is obtained from the stationary phase approximations for all the modes along the instanton path.[16]

Instead of referring to parabolic approximations at high temperatures and instanton paths at low temperatures, we adopt a simple approach to calculate the imaginary part of the barrier partition function for adiabatic processes. Motivated by the 2D quantum Boltzmann operator analyzed in recent work by Miller and co-workers,[4] we obtain $\mathrm{Im}\, Z_b$ from the structures of the 2D barrier free energy. Figure 2 illustrates the 2D barrier free energy profile $S(q,q') = -\ln\langle q|\exp[-\beta H/2]|q'\rangle$ of a symmetric Eckart potential which will be further discussed in Sec. III A. It demonstrates different saddle point structures above and below the crossover temperature, which give rise to the imaginary part of the barrier partition function. As the temperature increases above the crossover, the two saddle points on the 2D barrier free energy surface gradually merge into one saddle point. The 2D contours were used in recent work by Miller and co-workers[4] to extract the two dividing surfaces in the flux-flux correlation function. Here we analyze the saddle point structure of the 2D barrier free energy surface and calculate the barrier partition function with stationary phase approximations. At temperatures above the crossover, the free energy profile of the stable mode is steep, so a quadratic approximation is not accurate enough to approximate the integration over the stable mode. To overcome the inaccuracy of the quadratic approximation, we apply stationary phase approximations to the unstable modes along the stable coordinate and sum all contributions,

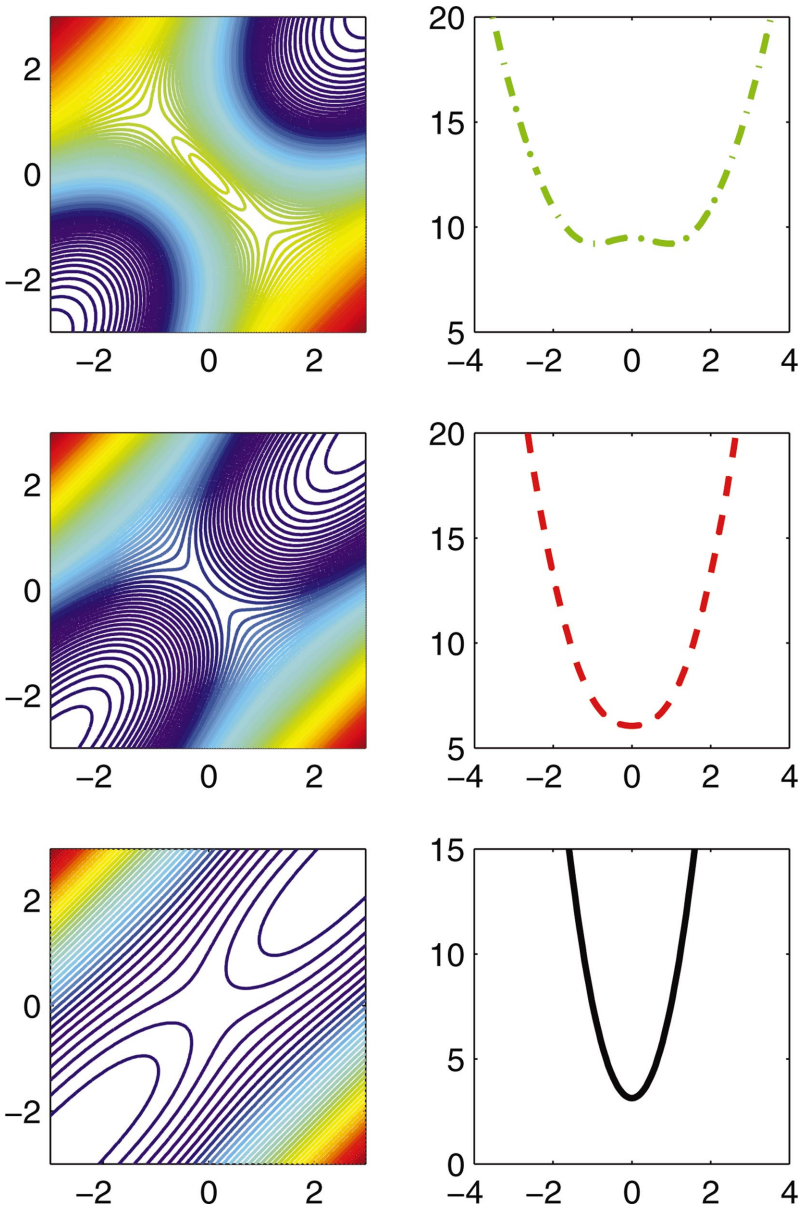

FIG. 2. (Color) Left column: Contour plots of 2D barrier free energy $-\ln\langle q|\exp[-\beta H/2]|q'\rangle$ for the symmetric Eckart potential at different temperatures, from top to bottom, $b=\beta\hbar\omega_b=12$, 2π, and 3, respectively. Right column: $-\ln\langle q|\exp[-\beta H/2]|q'\rangle$ along the off-diagonal directions of the corresponding contours.

$$\mathrm{Im}\, Z_b = \int dq_+ \sqrt{\frac{2\pi}{S''(q_+,q_-^{st})}}\, \exp[-2S(q_+,q_-^{st})], \tag{10}$$

where $q_+=(q+q')/2$ is the stable coordinate along the diagonal and $q_-=(q-q')/2$ is the unstable coordinate along the off-diagonal. The integrand is the stationary phase approximation to the unstable mode and the integration is along the stable coordinate. This scheme does not require the determination of the saddle points. When quadratic expansion at the saddle point is adequate, Eq. (10) reduces to the standard stationary phase approximation to the unstable modes at the saddle points.

The 2D barrier free energy method proposed here is a simple generalization of the barrier partition function concept[16,17] and applies to temperatures above and below the crossover. This method does not involve real-time calculations and can be implemented using available numerical algorithms such as numerical matrix multiplication (NMM) scheme, or path-integral Monte Carlo,[31] which is particularly useful for more complicated potentials where instanton paths are not easy to find. For dissipative systems, the quantum Boltzmann operator is averaged over all realizations of bath fluctuations. These numerical advantages render this method feasible for reaction processes that involve a large number of degrees of freedom. Further efforts along this direction should focus on the development of more accurate methods to extract the imaginary part of the barrier partition function.

C. Adiabatic and nonadiabatic instanton method

We now discuss the nonadiabatic instanton method which bridges the adiabatic and the nonadiabatic limits. The nonadiabatic coupling arises from the breakdown of the Born–Oppenheimer approximation of the electron transfer processes. The theoretical formalism for describing the nonadiabatic dynamics was first proposed by Pechukas, Freed, Tully, and Kapral, and developed by many others into surface hopping and various other numerical schemes for molecular dynamics (MD) simulations.[32–37] The nonadiabatic instanton theory is the imaginary-time analog of the Pechu-

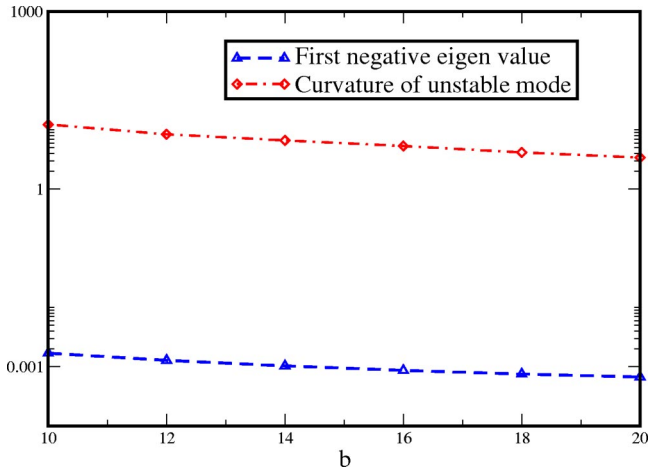

FIG. 3. Comparison of the curvature of the unstable modes at the saddle point of the 2D barrier free energy surface and the first negative eigenvalue of the instanton solution for the symmetric Eckart potential. Over a wide range of temperatures, they are proportional to each other.

kas formulation.[24–26] In the nonadiabatic limit, quantum reactive events arise from the crossing between electronic surfaces. The barrier partition function can be computed from the stationary phase approximation along the imaginary-time coordinate.[17] In the adiabatic limit, the reactive process is dominated by the lower adiabatic energy surface resulting from frequent crossings between the electronic surfaces. The barrier partition function in this limit is obtained from the stationary phase approximation to the spatial coordinates. Effectively, the nonadiabatic instanton approach rotates the stationary phase coordinate from the temporal axis in the nonadiabatic limit to the spatial axis in the adiabatic limit, which is illustrated in Fig. 1. The adiabatic instanton theory by Miller[2] relates the quantum reaction rate to the stationary phase approximation of the imaginary-time flux-flux correlation function in the adiabatic limit while the nonadiabatic instanton theory[17] demonstrate this relation in the nonadiabatic limit. Hence, the instanton approaches yield an important connection between the imaginary-time flux-flux correlation function concept and the barrier partition function concept.

The adiabatic instanton concept was originally introduced by Miller and has been applied extensively to dissipative and nondissipative systems.[2] To illustrate the connection that the instanton approach provides, we use the symmetric Eckart potential as an example. In agreement with discussions in the literature,[16,21] we notice the presence of an unstable mode of the instanton path, which corresponds to the negative eigenvalue. As we discussed earlier, the unstable mode also appears on the 2D barrier free energy surface. Both unstable modes give rise to the imaginary part of the barrier partition function. Figure 3 displays the curvature of the unstable mode at the saddle point of the 2D barrier free energy. It is proportional to the negative eigenvalue of the instanton path over a wide range of temperatures. This is a strong indication of the intrinsic connection between the 2D barrier free energy method and the instanton method. The eigenmode corresponding to the negative eigenvalue is shown in Fig. 4. The first negative mode is asymmetric with respect to the barrier top, and the first positive mode is a symmetric trajectory around the barrier top.

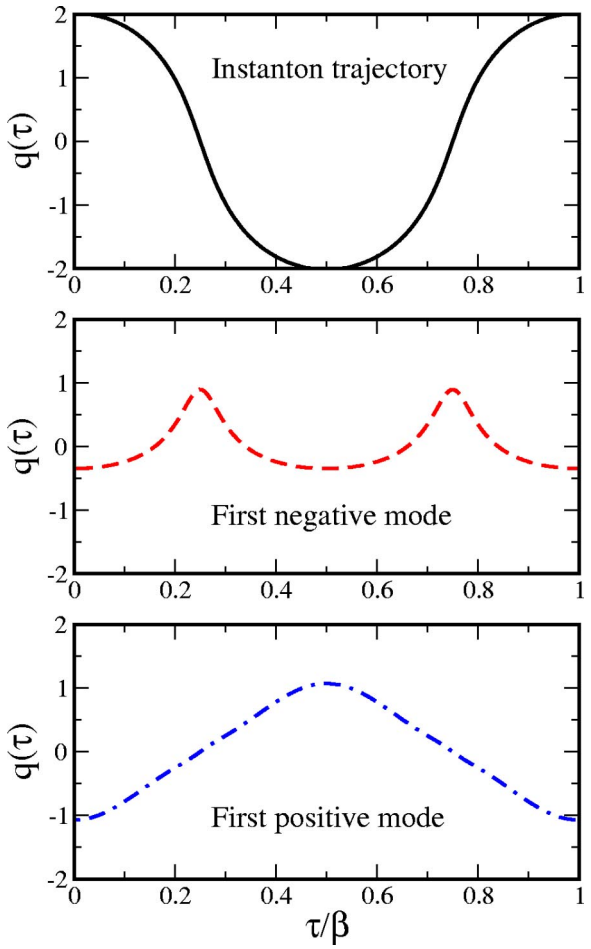

FIG. 4. The instanton trajectory, the first negative mode, and the first positive mode for the symmetric Eckart potential at $b=\beta\hbar\omega_b=24$.

III. ADIABATIC REACTIONS

To illustrate the stationary phase methods discussed in the preceding section, we present numerical results for quantum rate constants of several potentials in this section. For the nondissipative case, we investigate a 1D Eckart potential. For the dissipative case, we discuss a 1D Eckart potential and a double-well potential, both coupled to a harmonic bath. A study of the nonadiabatic rate constant of the spin-boson model is presented in Sec. IV.

In the presence of a potential barrier, the quantum flux operator measures the quantum reactive flux through the dividing surface q_n and is given as $\hat{F}_n=[\delta(q-q_n)\hat{p}+\hat{p}\delta(q-q_n)]/2m$, where $\hat{p}=-i\partial_q$ is the momentum operator. Carrying out the trace of Eq. (2) in the coordinate space yields

$$C_{ff}(\tau)Z_r=\left(\frac{1}{2m}\right)^2[\langle q_1|e^{-(\beta-\tau)H}|q_2\rangle'\langle q_1|e^{-\tau H}|q_2\rangle' + {}'\langle q_1|e^{-(\beta-\tau)H}|q_2\rangle'\langle q_1|e^{-\tau H}|q_2\rangle - {}'\langle q_1|e^{-(\beta-\tau)H}|q_2\rangle\langle q_1|e^{-\tau H}|q_2\rangle - \langle q_1|e^{-(\beta-\tau)H}|q_2\rangle'\langle q_1|e^{-\tau H}|q_2\rangle'], \quad (11)$$

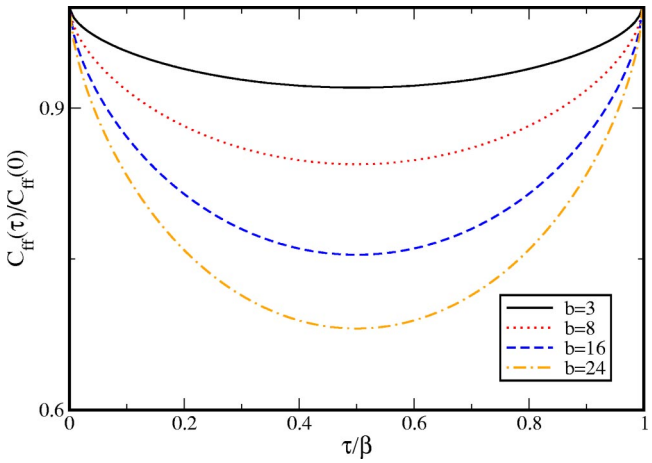

FIG. 5. The normalized imaginary-time flux-flux correlation function $C_{ff}(\tau)/C_{ff}(0)$ for the nondissipative Eckart potential at $b=3$, 8, 16, and 24.

where the left and the right primes represent spatial derivatives. This expression is given as Eq. (2.3) in Ref. 4. In our calculations, the dividing surface is defined at the top of the transition barrier, $q_1=q_2=0$, where reactants and products separate from each other.

A. Nondissipative case: 1D symmetric Eckart potential

Now we consider the nondissipative case using a 1D symmetric Eckart potential,

$$V(q) = V_0 \,\mathrm{sech}^2\left(\frac{q}{a}\right), \tag{12}$$

which has been studied by many other groups. We examine the optimized imaginary-time stationary phase method, the 2D barrier free energy method, and the consistency of these two methods. We use the same parameters as in Ref. 16, $2\pi V_0/\hbar\omega_b=12$, $a=1$, $m=1$, and $\hbar=1$. $b=\beta\hbar\omega_b$ is a dimensionless reduced temperature and $b=2\pi$ is the crossover temperature for the nondissipative case.

For the symmetric Eckart potential, the matrix element of $\exp[-H\tau]$ is evaluated using the NMM algorithm.[31] The imaginary-time flux-flux correlation functions at different temperatures are shown in Fig. 5. For the nondissipative Eckart potential, $-\ln C_{ff}(\tau)$ is well approximated by the quadratic reference discussed in Sec. III B. We notice that the non-Gaussian corrections at different temperatures are slightly different. In the crossover regime where $b\sim 2\pi$, $-\ln C_{ff}(\tau)$ at the stationary point $\tau=\beta/2$ is quadratic and the quartic term is negligible. At temperatures below the crossover, $b=8$, 16, and 24, the quartic term increases gradually and carries an opposite sign from the quadratic term. Hence, the correlation function becomes flatter. At $b=3$ above the crossover temperature, the quartic term also increases but carries the same sign as the quadratic term, consequently, the flux-flux correlation function becomes deeper.

Figure 2 illustrates 2D contour plots of the barrier free energy surface. Below the crossover temperature, two saddle points are found along the off-diagonal direction. The contour connecting these two saddle points essentially corresponds to the bounce trajectory, or the instanton path. As the temperature increases, the two saddle points merge into one, i.e., the instanton path converges to the barrier top. As shown in the left column of Fig. 2, at the temperature above the crossover, $b=3$, only one saddle point exists at the center of the contour plot. The crossover is better illustrated in the corresponding free energy profile along the off-diagonal directions in the right column of Fig. 2, where two minima of the stable mode merge gradually at higher temperatures.

The quantum correction factor $\Gamma=F_{qm}/F_{cl}$, defined as the ratio between the quantum reactive flux F_{qm} and the classical one $F_{cl}=e^{-\beta V_0}/2\pi\hbar\beta$, is tabulated in Table I. The instanton result Γ_{inst} is calculated with the method outlined in Ref. 16 and the exact result Γ_{exact} is computed with the ex-

TABLE I. Quantum correction factor for the symmetric Eckart potential.

$\beta\hbar\omega_b$	Γ_{exact} [a]	Γ_{inst} [b]	Γ_{bp} [c]	Γ_{flux} [d]
3	1.5	⋯	1.68	1.53
4	2.07	⋯	2.36	1.96
5	3.10	⋯	3.69	3.08
6	5.20	⋯	6.48	5.39
8	21.8	20.0	23.7	23.6
10	162	136	158	169
12	1973	1613	1796	1921
14	3.49×10^4	2.78×10^4	2.99×10^4	3.13×10^4
16	7.40×10^5	6.04×10^5	6.42×10^5	6.60×10^5
18	1.88×10^7	1.53×10^7	1.63×10^7	1.65×10^7
20	5.34×10^8	4.37×10^8	4.62×10^8	4.63×10^8
22	1.64×10^{10}	1.35×10^{10}	1.42×10^{10}	1.41×10^{10}
24	5.38×10^{11}	4.43×10^{11}	4.614×10^{11}	4.58×10^{11}
26	1.84×10^{13}	1.52×10^{13}	1.56×10^{13}	1.56×10^{13}
28	6.55×10^{14}	5.44×10^{14}	5.40×10^{14}	5.49×10^{14}
30	2.40×10^{16}	2.00×10^{16}	1.924×10^{16}	2.00×10^{16}

[a]Exact results calculated from expression in Ref. 38.
[b]Instanton calculation with the method in Ref. 16.
[c]Integrated stationary phase approximation to the 2D barrier free energy in Eq. (10).
[d]Optimized stationary phase approximation to the imaginary-time flux-flux correlation function in Eq. (6).

TABLE II. Quantum reactive flux for the dissipative symmetric Eckart potential.

$\beta\hbar\omega_b$	$\beta\hbar\lambda_0^{\ddagger}$	F_{inst}[a]	F_{bp}[b]	F_{flux}[c]
4	3.9	⋯	1.60×10^{-4}	1.51×10^{-4}
8	7.8	3.32×10^{-7}	3.04×10^{-7}	2.89×10^{-7}
12	11.7	4.25×10^{-9}	4.00×10^{-9}	3.97×10^{-9}
16	15.6	2.76×10^{-10}	2.56×10^{-10}	2.36×10^{-10}
20	19.5	3.53×10^{-11}	3.46×10^{-11}	2.95×10^{-11}
24	23.4	6.50×10^{-12}	6.41×10^{-12}	5.69×10^{-12}

[a]Instanton calculation with the method in Ref. 16.
[b]Integrated stationary phase approximation to the 2D barrier free energy in Eq. (10).
[c]Optimized stationary phase approximation to the imaginary-time flux-flux correlation function in Eq. (6).

pression in Ref. 38. Γ_{flux} represents the quantum correction factor calculated from the optimized stationary phase approximation to the imaginary-time flux-flux correlation function. Γ_{bp} is computed from the integrated stationary phase approximation to the 2D barrier free energy discussed in Sec. II B. The quantum correction factors from both stationary phase methods compare favorably with the instanton calculation and the exact results over a wide range of temperatures. These two methods proposed here show considerable improvements to the instanton calculations in the crossover regime and become almost identical to the instanton results at temperatures far below the crossover. Compared to the exact results Γ_{exact}, the optimized imaginary-time stationary phase method and the 2D barrier free energy method show an accuracy of ~10% at high temperature and ~20% at extremely low temperatures.

B. Dissipative case: 1D Eckart and double-well potentials

Now we discuss the calculation of quantum rate constants for the dissipative 1D potential. The full Hamiltonian is given by

$$H=\frac{p_q^2}{2m}+V(q)+\sum_j\left[\frac{p_j^2}{2m_j}+\frac{1}{2}m_j\omega_j^2\left(x_j-\frac{c_j}{m_j\omega_j^2}q\right)^2\right]. \tag{13}$$

Here, q is the system coordinate and x_j's describe a harmonic bath bilinearly coupled to the system coordinate. This Hamiltonian in Eq. (13) is widely employed to study the effects of condensed phase environments on charge transfer. The bath correlation is characterized by the spectral density $J(\omega)=\pi/2\Sigma_j(m_j\omega_j)^{-1}c_j^2\delta(\omega-\omega_j)$. In our calculation, we assume an ohmic spectral density with a frequency cutoff ω_c, i.e., $J(\omega)=\pi\hbar K\omega e^{-\omega/\omega_c}/2$, where K is the Kondo constant. In this section, the bath parameters are chosen to be $\omega_c=\omega_b$ and $K=0.1m\omega_b$. In the imaginary-time formulation, we integrate out the harmonic bath in Eq. (13) in a manner consistent with the Brownian oscillator model.[17] The action functional is

$$S=\int_0^\beta d\tau\left[\frac{1}{2}m\dot{q}^2+V(q)+\frac{1}{2}m\dot{\bar{x}}^2+\frac{1}{2}m\omega_0^2\left(\bar{x}-\frac{\lambda}{m\omega_0^2}q\right)^2\right]+\beta m\sum_{n>0}\Omega_n\hat{\gamma}(\Omega_n)|\hat{\bar{x}}_n|^2. \tag{14}$$

The last term is the influence functional, and $\hat{\bar{x}}_n=\beta^{-1}\int_0^\beta\exp[-i\Omega_n\tau]q(\tau)d\tau$ is the Fourier modes of the path $\bar{x}(\tau)$ at the Matsubara frequency $\Omega_n=2\pi n/\beta$. The frequency ω_0, the coupling constant λ, and $\hat{\gamma}(\Omega_n)$ are determined from the spectral density of the harmonic bath (see Appendix B in Ref. 17). The action functional in Eq. (14) provides a straightforward way to simulate the quantum dynamics. The presence of the system coordinate q in the action integral renders an explicit route to compute $\langle q|\exp(-H\tau)|q'\rangle$, which is necessary for computing the imaginary-time flux-flux correlation function and the barrier partition function. At each temperature, the Fourier modes of the trajectory $\bar{x}(\tau)$ are generated according to the Boltzmann distribution $\exp[-\beta m\Sigma_{n>0}\Omega_n\hat{\gamma}(\Omega_n)|\hat{\bar{x}}_n|^2]$. The quantum Boltzmann operator is computed accordingly and averaged over a number of bath trajectories. The imaginary-time flux-flux correlation function is computed using Eq. (11).

1. Eckart potential

For the dissipative Eckart potential, the bath averaged 2D barrier free energy surface (not shown here) displays similar features as the nondissipative case in Sec. III A. At temperatures below crossover, two saddle points are found along the off-diagonal direction; at high temperatures, these two saddle points merge into one. The quantum fluxes from the optimized imaginary-time stationary phase method and the 2D barrier free energy method are listed in Table II and compared with the adiabatic instanton approach outlined in Ref. 16. $\lambda_0^{\ddagger}$ is the Grote–Hynes frequency determined with Eq. (9). Clearly, both F_{bp} and F_{flux} agree closely with each other in the full temperature range. They also agree favorably with the instanton results below the crossover temperature. The deviation from the instanton calculation is within 15–20%. At low temperatures, the quantum fluxes obtained from the two stationary phase methods proposed in the present paper are consistently smaller than the instanton results. For the dissipative Eckart potential, instanton paths are difficult to calculate. In comparison, the two stationary phase methods in the present paper bypass the searching of instanton path and demonstrate reasonable accuracy at both high temperature regime and low temperature regime.

2. Double-well potential

The dissipative double-well potential is a practical model for proton transfer and electron transfer processes in condensed phases. By far there have been no direct applica-

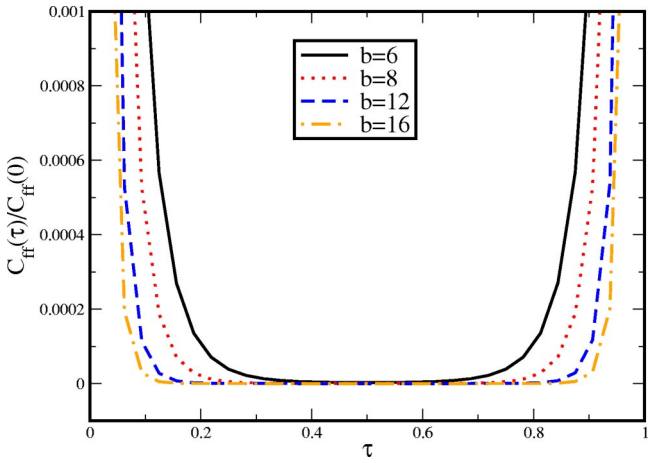

FIG. 6. The normalized imaginary-time flux-flux correlation function $C_{ff}(\tau)/C_{ff}(0)$ for the dissipative double-well potential at $b=6$, 8, 12, and 16.

tions of the flux-flux correlation function approach and the barrier partition function approach to the double-well systems. The present work provides a critical test of the optimized imaginary-time stationary phase method and the 2D barrier free energy method. The model Hamiltonian we study next has the same form as Eq. (13), except for the potential along the reaction coordinate which is a symmetric double well here,

$$V(q) = -a_1 q^2 + a_2 q^4. \tag{15}$$

In our calculation, $a_1=0.5$ and $a_2=0.015$ and the barrier frequency $\omega_b=1$. This set of parameters are consistent with the DW1 parameters used by Topaler and Makri.[8] As shown in Fig. 6, the flux-flux correlation function is quite flat and the flatness increases at lower temperatures. The optimized stationary phase approximation to the imaginary-time flux-flux correlation function requires accurate determination of the second and the fourth derivatives at the stationary point τ_{st}. We perform bath averages over 10^3-10^4 trajectories to obtain better accuracy and apply the optimized quadratic approximation.

Table III demonstrates that the quantum correction factor Γ_{flux} from the two stationary phase methods agree surprisingly well over the temperature range we studied. Even at low temperatures they differ by ~10%. The quantitative agreement with the instanton calculations is excellent at higher temperatures and slightly less favorable at lower temperatures. Compared to the real-time path-integral method such as quasiadiabatic path integral,[8] these two imaginary-time methods are simpler to compute numerically and yield the rate constant with similar accuracy. Yet, the stationary phase calculations do not contain the full dynamics. For example, they exclude the recrossing of the dividing surface observed in the real-time calculations.

IV. NONADIABATIC PROCESSES: SPIN-BOSON MODEL

The application of reaction rates for nonadiabatic condensed phase processes is an important step to test the methods discussed in Sec. II. The dynamic picture of such process involves transitions between two diabatic surfaces corresponding to the reactant and the product sites, respectively. The transition is induced by the coupling between the two diabatic surfaces. At low temperatures, this two-surface system reduces practically to a two-level system. Combination of the two surfaces and the bath leads to the famous spin-boson Hamiltonian,

$$H = \Delta\sigma_x + \sum_{j=1}^{N}\left[\frac{1}{2}m_j\dot{x}_j^2 + \frac{1}{2}m_j\omega_j^2\left(x_j - \frac{c_j}{m_j\omega_j^2}\sigma_z\right)^2\right], \tag{16}$$

where σ_i, $i=x,y,z$ is the Pauli spin matrix, Δ is one-half of the tunneling splitting. Despite its simplicity, the spin-boson model is widely employed to study the nonadiabatic dynamics of electron transfer reactions in biological systems and optical properties in one-dimensional conductors. Here we explore this problem using the optimized stationary phase approximation to the imaginary-time flux-flux correlation function.

For the spin-boson Hamiltonian, the flux operator in Eq. (1) reduces to $F=\Delta\sigma_y$. Consequently the imaginary-time flux-flux correlation function is

$$\begin{aligned} C_{ff}(\tau) &= \Delta^2 Z_r^{-1}\mathrm{Tr}\, e^{-\beta H}\sigma_y(\tau)\sigma_y(0) \\ &= \Delta^2 Z_r^{-1}\mathrm{Tr}\, e^{-H(\beta-\tau)}\sigma_y e^{-H\tau}\sigma_y. \end{aligned} \tag{17}$$

In our calculation, the spin-boson Hamiltonian is transformed into a two-level Brownian oscillator. The derivation can be found in Ref. 17 and the action term is given by

TABLE III. Quantum correction factor for the dissipative symmetric double-well potential.

$\beta\hbar\omega_b$	$\beta\hbar\lambda_0^{\ddagger}$	Γ_{inst} [a]	Γ_{bp} [b]	Γ_{flux} [c]
2.4	2.35	⋯	1.27	1.40
4	3.92	⋯	2.10	2.12
6	5.88	⋯	8.71	8.12
8	7.84	293	281	294
10	9.80	1.40×10^5	1.25×10^5	1.22×10^5
12	11.76	1.59×10^8	1.54×10^8	1.41×10^8
16	15.68	2.40×10^{14}	1.99×10^{14}	2.14×10^{14}

[a]Instanton calculation with the method in Ref. 16.
[b]Integrated stationary phase approximation to the 2D barrier free energy in Eq. (10).
[c]Optimized stationary phase approximation to the imaginary-time flux-flux correlation function in Eq. (6).

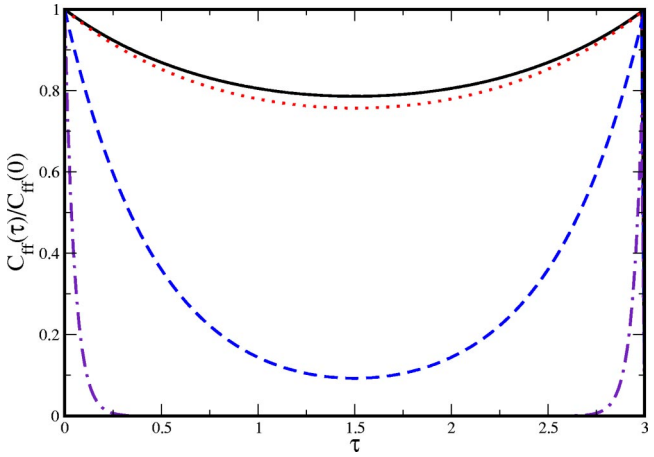

FIG. 7. The imaginary-time flux-flux correlation for the spin-boson model. The coupling constant varies from top to bottom, $\Delta=0.01$, 0.1, 1, and 10.

$$S=\int_0^\beta (\Delta\sigma_x-\lambda x\sigma_z)d\tau+\beta m\sum_{n>0}[\omega_0^2+\Omega_n^2+\omega_n\hat{\gamma}(\Omega_n)]\times|\tilde{x}_n|^2+\frac{\beta}{2}m\omega_0^2|\tilde{x}_0|^2+\frac{\beta\lambda^2}{2m\omega_0^2}, \tag{18}$$

where λ, ω_0, and $\hat{\gamma}(\Omega_n)$ are identical to the definitions in the dissipative Eckart potential. First, the Fourier modes of bath fluctuations are sampled from the Boltzmann distribution and the Euclidean path trajectory $x(\tau)$ is generated accordingly. Then, the imaginary-time path integral is propagated and the flux-flux correlation function of Eq. (18) is calculated along the trajectory $x(\tau)$. Finally the flux-flux correlation function is averaged over all possible realizations of bath fluctuations. To facilitate the comparison with the calculation in Ref. 17, in the present calculation we adopt the same set of parameters, $\hbar=1$, $\beta=3$, $\omega_c=1/\sqrt{2}$, and $K=0.25$.

The imaginary-time flux-flux correlations for different coupling constants at the temperature $\beta=3$ are plotted in Fig. 7. In the weak coupling limit, the flux-flux correlation function approaches the Golden rule result for the nonadiabatic limit,[17]

$$C_{ff}(\tau)=\exp\left\{-\frac{4}{\pi\hbar}\int\frac{J(\omega)d\omega}{\omega^2\sinh(\beta\hbar\omega/2)}\left[\cosh\frac{\beta\hbar\omega}{2}-\cosh\left(\frac{\beta\hbar\omega}{2}-\omega\tau\right)\right]\right\}. \tag{19}$$

In the large Δ limit, we notice that the imaginary-time flux-flux correlation function becomes flat, a behavior similar to that of the double-well potential in Fig. 6. In fact, in the large Δ limit, the energy gap between the two adiabatic surfaces of the spin-boson model is large compared to the thermal energy k_BT. Then, there is little contribution from the upper energy surface and the quantum dynamics is completely dominated by the lower energy surface, giving the adiabatic limit of the spin-boson Hamiltonian. Considering the presence of the diabatic surfaces of reactants and products, the adiabatic limit of the spin-boson Hamiltonian is similar to a double-well potential. This explains the close resemblance of the imaginary-time flux-flux correlation function at large Δ

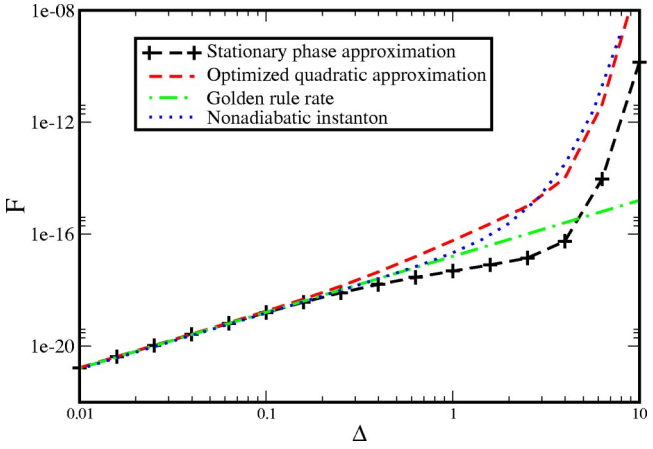

FIG. 8. The quantum flux of the spin-boson model calculated with the optimized imaginary-time stationary phase method in Eq. (6). The dotted-dashed line is the Golden rule rate. The dotted line is the nonadiabatic instanton result.

to the dissipative double-well potential. When the correlation function is flat, the quadratic stationary phase approximation is inadequate for time integration. To incorporate the non-Gaussian effects, we use the optimized quadratic approximation discussed in Sec. II A.[28]

The quantum fluxes are plotted as a function of the coupling constant Δ in Fig. 8. The quantum flux obtained from the optimized imaginary-time stationary phase method is in excellent agreement with the nonadiabatic instanton calculations in Ref. 17. In the weak coupling limit, the quantum rate approaches the Golden rule rate in the nonadiabatic limit, which is proportional to Δ^2.[17,39] In the strong coupling limit, the spin-boson rate constant approaches the adiabatic rate, which has an exponential dependence on the coupling constant, $K\propto e^{\beta\Delta}$. Nevertheless, the optimized imaginary-time stationary phase method differs slightly from the nonadiabatic instanton results at the intermediate coupling strengths. We observed that the non-Gaussian correction factor in Eq. (6) becomes significant at larger Δ, indicating a substantial deviation from the quadratic reference system. This can be seen from the difference between the plain stationary phase approximation and the optimized quadratic approximation in Fig. 8. Overall, the optimized quadratic approximation has improved dramatically the standard stationary phase approximation and more advanced numerical techniques have to be developed to overcome the inaccuracy introduced by the quadratic reference system.

V. CONCLUDING REMARKS

Two stationary phase methods, the optimized stationary phase approximation to the imaginary-time flux-flux correlation function and the integrated stationary phase approximation to the 2D barrier free energy, provide a practical way to compute the quantum reaction rate in complex systems. Unlike quantum transition state theory which diverges at low temperatures, or the instanton theory which is valid below the crossover temperature, these two stationary phase methods work equally well for high and low temperatures, as well as in the crossover regime. In the optimized imaginary-time

stationary phase method, we employ the optimized quadratic approximation to overcome the inaccuracy of the standard stationary phase approximation, which extends the stationary phase approach by Wolynes[5] to both adiabatic and nonadiabatic processes. In the 2D barrier free energy method, the quantum rate is obtained from the integrated stationary phase approximations to the spatial coordinates on the 2D barrier free energy surface. This method is applicable to adiabatic processes only. The nonadiabatic instanton approach effectively rotates the stationary phase axis from the imaginary-time coordinate in the nonadiabatic limit to the spatial coordinates in the adiabatic limit, providing a natural unification between these two stationary phase approximations. In comparison, these two stationary phase methods are numerically simpler and computationally feasible for complex systems.

In the present paper, we extensively test the general applicability and reliability of the optimized imaginary-time stationary phase method and the 2D barrier free energy method. For the adiabatic systems we studied, these two stationary phase methods agree at all temperatures studied and match the instanton results with reasonable accuracy in the low-temperature region. For the nonadiabatic spin-boson model, the optimized imaginary-time stationary phase method agrees with the nonadiabatic instanton result and interpolates well between the nonadiabatic and the adiabatic limits. Considering the conceptual clarity and the numerical simplicity of the stationary phase approximations, further efforts along this direction should be focused on developing more dependable approximations to evaluate or extract the quantum reactive flux. The optimized stationary phase approximation to the imaginary-time flux-flux correlation function is generally applicable to both adiabatic and nonadiabatic processes while the 2D barrier free energy method is particularly easy to use for adiabatic processes. With comparable accuracy to other available methods, these two stationary phase approximations are numerically faster. Applications to higher dimensional complex systems are necessary to corroborate the validity and the numerical advantages of these methods.

ACKNOWLEDGMENTS

This research was supported by the NSF Career Award (Grant No. Che-0093210) and the Petroleum Research Fund administrated by the American Chemical Society. J.C. is a recipient of the Camille Dreyfus Teacher-Scholar Award.

[1] P. Hänggi, P. Talkner, and M. Borkovec, Rev. Mod. Phys. **62**, 251 (1990).
[2] W. H. Miller, J. Chem. Phys. **62**, 1899 (1975).
[3] W. H. Miller, S. D. Schwartz, and J. W. Tromp, J. Chem. Phys. **79**, 4889 (1983).
[4] W. H. Miller, Y. Zhao, M. Ceotto, and S. Yang, J. Chem. Phys. **119**, 1329 (2003).
[5] P. G. Wolynes, J. Chem. Phys. **87**, 6559 (1987).
[6] P. G. Wolynes, J. Chem. Phys. **86**, 1957 (1987).
[7] T. J. Park and J. C. Light, J. Chem. Phys. **88**, 4897 (1988).
[8] M. Topaler and N. Makri, J. Chem. Phys. **101**, 7500 (1994).
[9] D. Thirumalai and B. J. Berne, Comput. Phys. Commun. **63**, 415 (1991).
[10] D. Kim, J. D. Doll, and J. E. Gubernatis, J. Chem. Phys. **106**, 1641 (1997).
[11] D. Kim, J. D. Doll, and D. L. Freeman, J. Chem. Phys. **108**, 3871 (1998).
[12] E. Rabani, G. Krilov, and B. J. Berne, J. Chem. Phys. **112**, 2605 (2000).
[13] A. A. Golosov, D. R. Reichman, and E. Rabani, J. Chem. Phys. **118**, 457 (2003).
[14] J. S. Langer, Ann. Phys. (N.Y.) **41**, 108 (1967).
[15] I. Affleck, Phys. Rev. Lett. **46**, 388 (1981).
[16] J. Cao and G. A. Voth, J. Chem. Phys. **105**, 6856 (1996).
[17] J. Cao and G. A. Voth, J. Chem. Phys. **106**, 1769 (1997).
[18] P. G. Wolynes, Phys. Rev. Lett. **47**, 968 (1981).
[19] G. A. Voth, D. Chandler, and W. H. Miller, J. Chem. Phys. **91**, 7749 (1989).
[20] G. A. Voth, J. Phys. Chem. **97**, 8365 (1993).
[21] J. L. Liao and E. Pollak, J. Chem. Phys. **116**, 2718 (2002).
[22] C. G. Callan and S. Coleman, Phys. Rev. D **16**, 1762 (1977).
[23] R. F. Dashen, B. Hasslacher, and A. Neveu, Phys. Rev. D **10**, 4114 (1974).
[24] J. Cao, C. Minichino, and G. A. Voth, J. Chem. Phys. **103**, 1391 (1995).
[25] C. D. Schwieters and G. A. Voth, J. Chem. Phys. **108**, 1055 (1998).
[26] S. J. Jang and J. Cao, J. Chem. Phys. **114**, 9959 (2001).
[27] J. Cao and B. J. Berne, J. Chem. Phys. **92**, 7531 (1990).
[28] J. Cao and G. A. Voth, J. Chem. Phys. **102**, 3337 (1995).
[29] R. F. Grote and J. T. Hynes, J. Chem. Phys. **73**, 2715 (1980).
[30] E. Pollak, J. Chem. Phys. **85**, 865 (1986).
[31] B. J. Berne and D. Thirumalai, Annu. Rev. Phys. Chem. **37**, 401 (1986).
[32] P. Pechukas, Phys. Rev. **181**, 166 (1969).
[33] P. Pechukas, Phys. Rev. **181**, 174 (1969).
[34] M. F. Herman and K. F. Freed, J. Chem. Phys. **78**, 6010 (1983).
[35] J. C. Tully and R. K. Preston, J. Chem. Phys. **55**, 562 (1972).
[36] F. J. Webster, P. J. Rossky, and R. A. Friesner, Comput. Phys. Commun. **63**, 494 (1991).
[37] R. Kapral and G. Ciccotti, J. Chem. Phys. **110**, 8919 (1999).
[38] H. S. Johnston, *Gas Phase Reaction Rate Theory* (The Ronald Press Company, New York, 1966).
[39] U. Weiss, *Quantum Dissipative Systems* (World Scientific, Singapore, 1999).